frontiers | Frontiers in Earth Science

ORIGINAL RESEARCH
published: 31 May 2022
doi: 10.3389/feart.2022.893969

Experimental Study on the Effect and Mechanism of Chemical Stimulation on Deep High-Temperature Granite

Zhenpeng Cui[1,2], *Shuantong Shangguan*[3], *Fabrizio Gherardi*[4], *Xiaofei Qi*[3], *Jianan Xu*[1,2], *Siqing He*[1,2] *and Bo Feng*[1,2]*

[1]Key Laboratory of Groundwater Resources and Environment, Ministry of Education, Jilin University, Changchun, China, [2]Engineering Research Center of Geothermal Resources Development Technology and Equipment, Ministry of Education, Jilin University, Changchun, China, [3]No.2 Exploration Team, Hebei Bureau of Coal Geological Exploration, Xingtai, China, [4]Institute of Geosciences and Earth Resources, Italy National Research Council, Pisa, Italy

Chemical stimulation has been increasingly applied to improve the performance of geothermal reservoirs since early 1980s. The potential for the successful application of this technique to high-temperature reservoirs hosted in granitic rocks is still uncertain, and one of the keys to assess this potential is to investigate experimentally the geochemical reactivity induced *via* chemical stimulation on relevant rock specimens. On this premise, we combined high-temperature and high-pressure dynamic simulation and static corrosion experiments to explore the effect of different chemical stimulants on the permeability of granite samples from the Baimiao formation (Hebei Province, China). Experimental results show that NaOH-dominated alkaline stimulants cause only weak dissolution patterns on primary feldspar and quartz, and they do not sensitively affect the original amount of chlorite. The overall effect is a negligible enhancement of the original permeability of all the granite specimens analyzed. Conversely, a large increase in permeability is observed when an acid mixture of 10wt% HCl + 1.5wt% HF is used as a stimulant, with an observed maximum magnifying effect of about 27 times, due to the effective dissolution of feldspar and chlorite. Though quartz appears not to be affected by dissolution, a relatively large amount of secondary neo-formed amorphous silica is also documented.

Keywords: laboratory experiment, mechanism analysis, enhanced geothermal system, chemical stimulation, permeability modification, secondary precipitation

OPEN ACCESS

Edited by:
Wenjing Lin,
Chinese Academy of Geological Sciences, China

Reviewed by:
Xianzhi Song,
China University of Petroleum, Beijing, China
Yanlong Kong,
Chinese Academy of Sciences (CAS), China

***Correspondence:**
Bo Feng
fengbo234@126.com

Specialty section:
This article was submitted to Geochemistry, a section of the journal Frontiers in Earth Science

Received: *11 March 2022*
Accepted: *01 April 2022*
Published: *31 May 2022*

Citation:
Cui Z, Shangguan S, Gherardi F, Qi X, Xu J, He S and Feng B (2022) Experimental Study on the Effect and Mechanism of Chemical Stimulation on Deep High-Temperature Granite. Front. Earth Sci. 10:893969. doi: 10.3389/feart.2022.893969

1 INTRODUCTION

Owing to the latest generation technology, geothermal energy is considered clean, renewable, and economically exploitable on a large scale (e.g., among many others, Liao et al., 2006). Due to its huge reserves and wide distribution, geothermal energy has become one of the most important alternative new energy sources after coal and oil and has attracted extensive research and development all over the world (Xu, 2005). It is estimated that if just 1% of the geothermal potential in the earth's crust might be fully utilized, the world energy requirement for 2,800 years would be provided at the current energy consumption rate (Olasolo et al., 2016; Alegria et al., 2022).

Enhanced geothermal systems (EGSs) are engineered geothermal reservoirs developed to commercially mine heat from hot rocks that have limited pathways through which operation fluids can flow (e.g., among many others, Wang et al., 2020). The key to the successful operation of

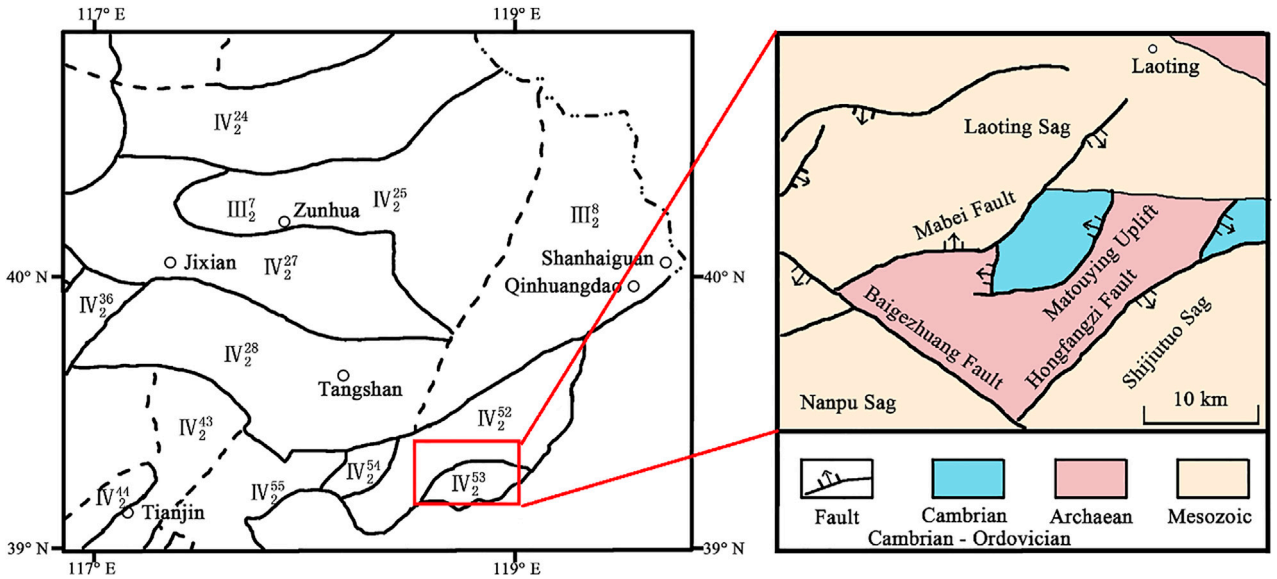

FIGURE 1 | Structural location of the study area. III_2^7: Malanyu compound anticline; III_2^8: Shanhaiguan anticline; IV_2^{24}: Kuancheng concave fold bundle; IV_2^{25}: Zunhua fornix fold bundle; IV_2^{27}: Jixian concave fold bundle; IV_2^{28}: Kailuan depressional platform; IV_2^{36}: Dachang uplift; IV_2^{43}: Panzhuang depression; IV_2^{44}: Dacheng depression; IV_2^{52}: Nanpu uplift; IV_2^{53}: Matouying uplift; IV_2^{54}: Baigezhuang uplift; IV_2^{55}: Beitang depression.

the EGS lies in the artificial creation of a network of hydraulically transmissive fractures in the low permeability rock (reservoir reconstruction), with the ultimate goal to establish a large volume of the water storage layer, to increase the contact area between the fluid for heat exchange and the high-temperature rock, and to establish a good hydraulic connection between the injection well and production well (e.g., Xu et al., 2018; Feng et al., 2019). At present, the main methods of stimulating artificial reservoirs include hydraulic fracturing, thermal stimulation, and chemical stimulation (Wang et al., 2012). Among them, hydraulic fracturing and thermal stimulation have some problems in practical application, such as unsatisfactory reconstruction effect, poor stability, and ease in inducing microseisms. As a kind of soft stimulation technology, chemical stimulation has the potential to enhance reservoir permeability without the abovementioned drawbacks associated with hydraulic and thermal stimulation practices (Luo et al., 2018).

Chemical stimulation relies on the injection of chemically reactive agents at a pressure lower than the formation fracture pressure. Reservoir permeability enhancement occurs through mineral dissolution. It is a method originally developed for, and widely applied in, oil and gas applications (Smith and Hendrickson, 1965; Economides and Nolte, 1989; Schechter, 1992; Liu et al., 2016). Any conventional chemical stimulation program is usually divided into three stages: pre-flush, main flush, and post-flush (Portier et al., 2009; Yang, 2012). The main purpose of the pre-flush stage is to prepare for the main stimulation stage by dissolving and expelling some mineral components (for example carbonates) that have the potential to hamper the stimulation effect *via* geochemical buffering. The main purpose of the post-flush stage is to keep the permeability of the reservoir stable by discharging the residual acid (or alkali) and reactive minerals in the fracture.

The effectiveness of the chemical stimulation sensitively depends on the type of stimulants and their reaction mechanism with formation minerals (Perthuis et al., 1989; Davies et al., 1994). The chemical agents commonly used in EGS practices comprise acidic and alkaline compounds. Acidic stimulants typically include conventional and retarded acid systems, mud acid (HCl + HF), chelating acids, and CO_2 (Portier and Vuataz, 2010; Yang, 2012). Alkaline stimulants mainly include NaOH, Na_2CO_3, and chelating bases (Evanoff et al., 1997; Sarda, 1977). Recent research developments have focused on the experimental study of the impact of HF and organic acid mixtures on the structure of sandstone rocks (Yang, 2012), and on the integration of experimental and numerical techniques to assess the performance of CO_2 as a chemical stimulant in EGS reservoirs (Na et al., 2014). In addition, the influence of high-concentration mud acid on the hydraulic characteristics of fractured granite has been recently addressed (Luo et al., 2018). The results of these laboratory experiments show that the permeability of fractured granite samples can be greatly improved after the static reaction with high-concentration mud acid. Finally, the reaction kinetics between soil acid and granite has been explored in some detail through static dissolution experiments and numerical modeling (Yue et al., 2020).

Despite all these efforts, the performance of chemical stimulation practices under field conditions still remain highly uncertain and inherently difficult to predict. For instance, both duration and mode of interaction between chemical stimulants and rocks are expected to be significantly different from laboratory conditions due to the inherently high complexity of

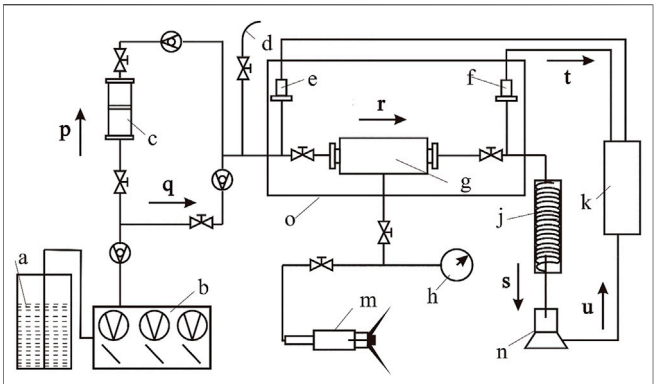

FIGURE 2 | Structure diagram of the core flow instrument. a, Ultrapure water; b, constant speed and pressure pump; c, intermediate container; d, safety valve; e, inlet pressure; f, outlet pressure; g, core holder; h, confining pressure gage; j, condenser; k, data acquisition device; m, hand pump; n, electronic balance; o, blast oven; p, ultrapure water; q, chemical stimulant; r, injected fluid; s, residual liquid; t, pressure data; u, velocity data.

the spatial distribution of fractures at the reservoir scale and the large variability of fluid–rock interaction conditions. For example, at the end of the injection stage, part of the chemical stimulant is expected to remain in the reservoir fractures, providing the driving force for additional mineral/dissolution processes, which may have side effects on reservoir reconstruction.

To account for all these complexities, in this study, we performed dynamic and static experiments on granite samples under high-temperature and high-pressure conditions. Dynamic experiments were carried out to explore the effect of different chemical stimulants during the injection phase. A set of prolonged static corrosion experiments were carried out under the same reaction conditions to explore "residual" reaction mechanisms likely associated with the late stages of the chemical stimulation. Granite rocks of the Baimiao formation of the Archean Dantazi Group in the Matouying uplift area (Hebei Province, China) are the target of our experiments.

2 GEOLOGICAL AND GEOTHERMAL SETTING

The study area is located in the Matouying uplift area in the eastern part of Hebei Province, China (**Figure 1**). The Matouying uplift is a secondary structural unit in the northern margin of Huanghua depression of North China fault depression, surrounded by Laoting depression, Nanpu depression, and Shijiutuo depression, bordering Bozhong depression in the southeast and Yanshan fold belt in the north. Both mantle-derived heat and radioactive heat contribute to the terrestrial heat flow of the study area. Deep and large faults exist in the region, which act as preferential pathways for heat and mass ascent through the crust (e.g., Cangdong and Tanlu fault zones; Zhang et al., 2020).

Regional geology is characterized by the occurrence of lithologies of the Archean to Quaternary age. Cenozoic formations, mainly represented by variable grain-sized sandstones and clay rocks, act as the local caprock. The Matouying uplift is characterized by a heat flow larger than 75 mW/m^2, slightly higher than the global average heat flow value (Wang et al., 1990), associated with a geothermal gradient generally comprised between 30 and 50°C/km, and up to a maximum of about 70°C/km in the middle of the area (Shangguan, 2017; Qi et al., 2020).

The target reservoir of this study is the metamorphosed granite of Baimiao formation of the Archean Dantazi Group. The surface of this granite is between 1200 and 1900 m b.g.l, whereas the bottom is generally deeper than 4000 m b.g.l, which corresponds to an approximate thickness of 1500–2,500 m. The maximum temperature is slightly above 150°C, which is considered appealing for geothermal applications (Qi et al., 2018). The main mineralogical constituents are K-feldspar (30%), plagioclase (33%), quartz (20%), chlorite (15%), and biotite (2%).

3 METHODS

3.1 Dynamic Simulation Experiment

3.1.1 Experimental Purpose and Principle

This experiment aims at reproducing the dynamics of the injection phase of the chemical stimulant in the reservoir. The variations in the equivalent permeability of the rock specimens were used as the master variable to monitor the impact of the stimulants on the granite structure. The equivalent permeability was calculated by applying **Eq. 3** along with instantaneous information on pressure and liquid outflow collected during the experiment. **Eq. 3** was deduced from Darcy's Law (**Eq. 1**) and the relationship between permeability and permeability coefficient (**Eq. 2**).

$$Q = K \times A \times \frac{H_1 - H_2}{L}, \tag{1}$$

$$k = K\frac{\mu}{\rho g}, \tag{2}$$

$$k = \frac{Q\mu L}{A(P_1 - P_2)}. \tag{3}$$

In **Eqs. (1–3)**, k [m^2] is the equivalent permeability, Q [m^3/s] is the liquid flow through the core, μ [Pa·s] is the dynamic viscosity coefficient of the liquid, L [m] is the core length, A [m^2] is the cross-sectional area of the core, P_1 [Pa] and P_2 [Pa] are, respectively, the inlet and outlet port pressure, K [m/d] is the permeability coefficient, H_1 [m] and H_2 [m] are the inlet and outlet head, respectively, ρ [kg/m^3] is the liquid density, and g [m/s^2] is the acceleration of gravity.

Further insights on the reaction mechanisms induced by the different stimulants were obtained by monitoring the chemical concentration of K^+, Na^+, Mg^{2+}, Al^{3+}, and soluble silicon. By applying mass conservation principles, the degree of progress of different mineral dissolution/precipitation processes was assessed with respect to the stoichiometry of the primary minerals.

3.1.2 Experimental Equipment and Samples

This experiment was carried out with the high-temperature and high-pressure core flow instrument of **Figure 2**. This instrument comprises a constant speed and pressure pump, a blast oven, an

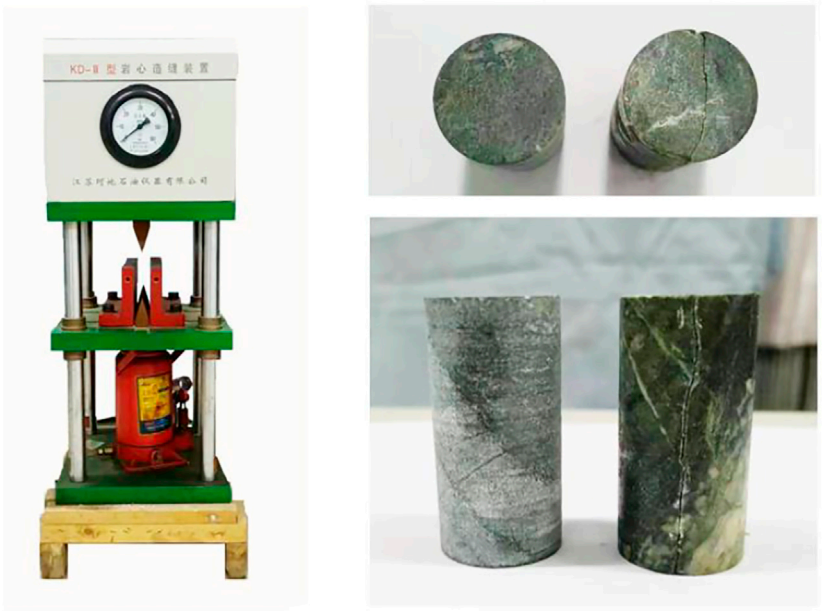

FIGURE 3 | Device for artificially creating fractures and cores before and after splitting.

intermediate container, a core holder, a hand pump, a condenser, and a data acquisition device (**Figure 2**). The constant speed and constant pressure pump is used to control the flow rate or injection pressure of the fluid. The blast oven, the core holder, and the hand pump are used to simulate temperature and pressure conditions in the actual EGS reservoir. The intermediate container is used to complete the transition between chemical stimulants and ultrapure water. The condenser is used for the collection of the residual liquid. The data acquisition device is used to record instantaneous flow information and pressure at the inlet and outlet ports.

Rock specimens used in the tests were cylindrical samples with 2.5 cm diameter and 5 cm length artificially fractured before the experiment. The device used to fracture the rock specimens is shown in **Figure 3**, along with cores before and after fracturing.

3.1.3 Experimental Schemes

NaOH and mud acid (HCl + HF) were selected as reference stimulants, and their relative concentration was set according to relevant literature (Na et al., 2017; Guo et al., 2020). In order to avoid excessive secondary precipitation in the reaction systems when alkaline chemical stimulants are used, two stable and efficient chelators, ATMP and PESA, were added in schemes D1 and D2, respectively, to chelate the metal ions produced by chemical stimulation and inhibit secondary precipitation. In scheme D3, HCl mainly plays the role of maintaining low pH. No chelating agent was added in this scheme because metal ion chelating agents are not effective under low pH conditions (**Table 3**).

Ultrapure water was used in the pre-flush and post-flush stages and main flush of the blank control experiment. The duration of the core flow experiment is 3 h in which the pre-flush stage and post-flush stage last 0.5 h as the main flush stage lasts 2 h. To make the reaction conditions closer to the actual formation, the temperature is set at 150°C, the confining pressure is set at 10 MPa, and the injection flow rate is set at 2 ml/min.

The artificially fractured cores were wrapped by a rubber sleeve resistant to high temperature and acid–base corrosion and transferred into the core holder. Ultrapure water was injected at a constant speed as soon as the temperature inside the oven and the pressure were stabilized at 150°C and 10 MPa, respectively. The valves of the intermediate container were rotated at 0.5 and 2.5 h to complete the transition between ultrapure water and the stimulant. The instantaneous data of inlet and outlet port pressure and liquid outflow were collected in the whole process of the experiment, and the discharged liquid was collected at 0.5, 1, 1.5, 2, 2.5, and 3 h, and each sampling lasts for 0.5 h.

3.2 Static Corrosion Experiment

3.2.1 Experimental Purpose and Principle

Chemical stimulants are expected to stay longer within the fractures under field conditions compared to laboratory conditions. Chemical agents remaining in the fractures likely continue to react with reservoir rocks, possibly causing additional precipitation/dissolution processes that might negatively affect reservoir reconstruction. On this premise, a number of static dissolution experiments were performed under the same P,T conditions of the dynamic experiment to explore geochemical reactivity over longer timescales.

3.2.2 Experimental Equipment and Samples

Static experiments were carried out with a high-temperature, high-pressure reactor (ML-0.3). As shown in **Figure 4**, the overall structure of the instrument can be divided into three parts:

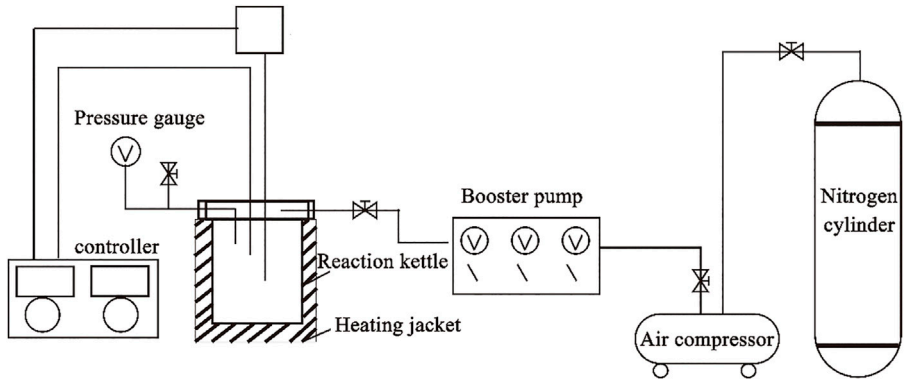

FIGURE 4 | Structural diagram of the high-temperature and high-pressure reactor.

TABLE 1 | Scheme of the dynamic simulation experiment.

Scheme number	Pre-flush (0.5 h)	Main flush (2 h)	Post-flush (0.5 h)
Blank scheme	Ultrapure water	Ultrapure water	Ultrapure water
D1	Ultrapure water	10wt% NaOH+3wt% ATMP	Ultrapure water
D2	Ultrapure water	10wt% NaOH+1wt% PESA	Ultrapure water
D3	Ultrapure water	10wt% HCl+1.5wt% HF	Ultrapure water

TABLE 2 | Schemes of the high-temperature and high-pressure static corrosion experiment.

Scheme number	Formula of the stimulant	Mass ratio (stimulant to rock powder)	Sampling time point (h)
S1	10wt% NaOH + 3wt% ATMP	10:1	1, 2, 4, 6, 12
S2	10wt% NaOH + 1wt% PESA	10:1	1, 2, 4, 6, 12
S3	10wt% HCl + 1.5wt% HF	10:1	1, 2, 4, 6, 12

heating device, pressurization system, and reactor body. The heating device comprises a heating sleeve and a controller. The pressurization system consists of a booster pump, an air compressor, and a nitrogen cylinder. The main body of the reactor is Hastelloy, which has strong corrosion resistance. The standard capacity of the reactor is 500 ml, and the maximum working temperature and pressure are 400°C and 12 MPa, respectively. Granite samples were pulverized and sieved (100–200 mesh), and the rock powder was sub-packed.

3.2.3 Experimental Schemes

For the sake of consistency, the same T,P conditions of the dynamic experiment (150°C and 10 MPa) were applied. To ensure that the content of the chemical stimulant was enough to maintain full contact between the sample and the stimulant over relatively long times, the chemical stimulant and the prepared rock powder were mixed in the mass ratio 10:1. During the experiment, the autoclave was opened for sampling after 1, 2, 4, 6, and 12 h reaction time, and the contents of K+, Na+, Mg2+, Al3+, and soluble silicon in the residual acid/alkaline were analyzed. The amounts of dissolved/precipitated minerals, along with the variations in the chemical composition of the reaction residue, were measured after washing, filtering, and drying. XRD mineral composition analysis and scanning electron microscope test of the rock powder residue after the reaction were carried out according to the experimental scheme of **Table 2**.

4 RESULTS AND DISCUSSION

4.1 Dynamic Effect of Chemical Stimulants on Permeability of Cores

Time variations of the equivalent permeability of the cores are shown in **Figure 5** for different experimental setups, during the dynamic experiment. The main features of the dynamic experiment are listed below.

During the whole process of injection of ultrapure water, the equivalent permeability of the core gradually decreased and finally approached a plateau, suggesting that ultrapure water had no effect on improving core permeability.

In addition, the NaOH-dominated alkaline chemical stimulants had minimal impact on the permeability of the specimen. Under both D1 and D2 conditions, the permeability was not sensitively modified during the early and late stages of the main flush, and just some abrupt changes were observed during the intermediate stage, after about 1 h. Though some larger

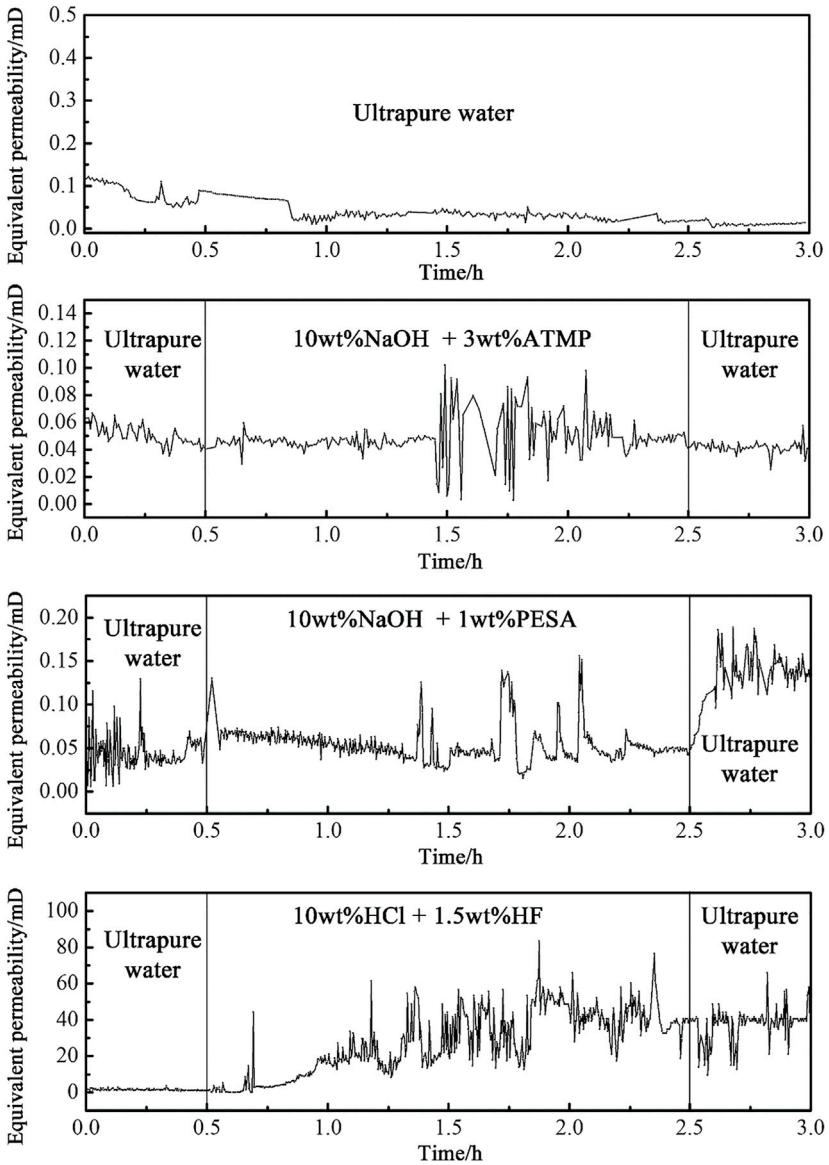

FIGURE 5 | Change of equivalent permeability of the cores with time.

increase in permeability was observed under D2 conditions, this result was interpreted as an evidence for the occurrence of similar reaction mechanisms under the two stimulation schemes.

The use of the alkaline 10wt% NaOH + 3wt% ATMP agent, after the completion of the flushing with ultrapure water, caused the permeability to slightly decrease below the average value of the pre-flush stage. The injection of the 10wt% NaOH + 1wt% PESA stimulant led to an increase of the equivalent permeability up to a plateau at about 2.83 times the initial value. Compared with 10wt% NaOH + 3wt% ATMP, 10wt% NaOH + 1wt% PESA played a positive role in improving equivalent permeability, but the effect was still not obvious. In this scheme, the improvement of equivalent permeability mainly occurred in the post-flush stage, and there was no stable and continuous increase during the main flush. Based on these evidences, we conclude that the 10wt% NaOH + 1wt% PESA system did not cause effective mineral corrosion in the fracture. The increase of equivalent permeability in the post-flush stage was due to the change of injected fluid viscosity and the scouring of ultrapure water on the secondary precipitated particles produced in the main flush stage.

Conversely, the application of the 10wt% HCl + 1.5wt% HF system led to a more significant and rapid impact on core equivalent permeability, compared to the alkaline system. In this scheme, the time pattern of the equivalent permeability was characterized by a steady increase after 0.4 h of the main flush stage, with significant fluctuations before and after 1 h reaction time, and with steady, high-permeability values after 1.6 h. During the post-flush stage, the equivalent permeability quickly recovered the level at the end of the main flush stage, before stabilizing at about 39.41mD, that is, more than 27 times the initial equivalent

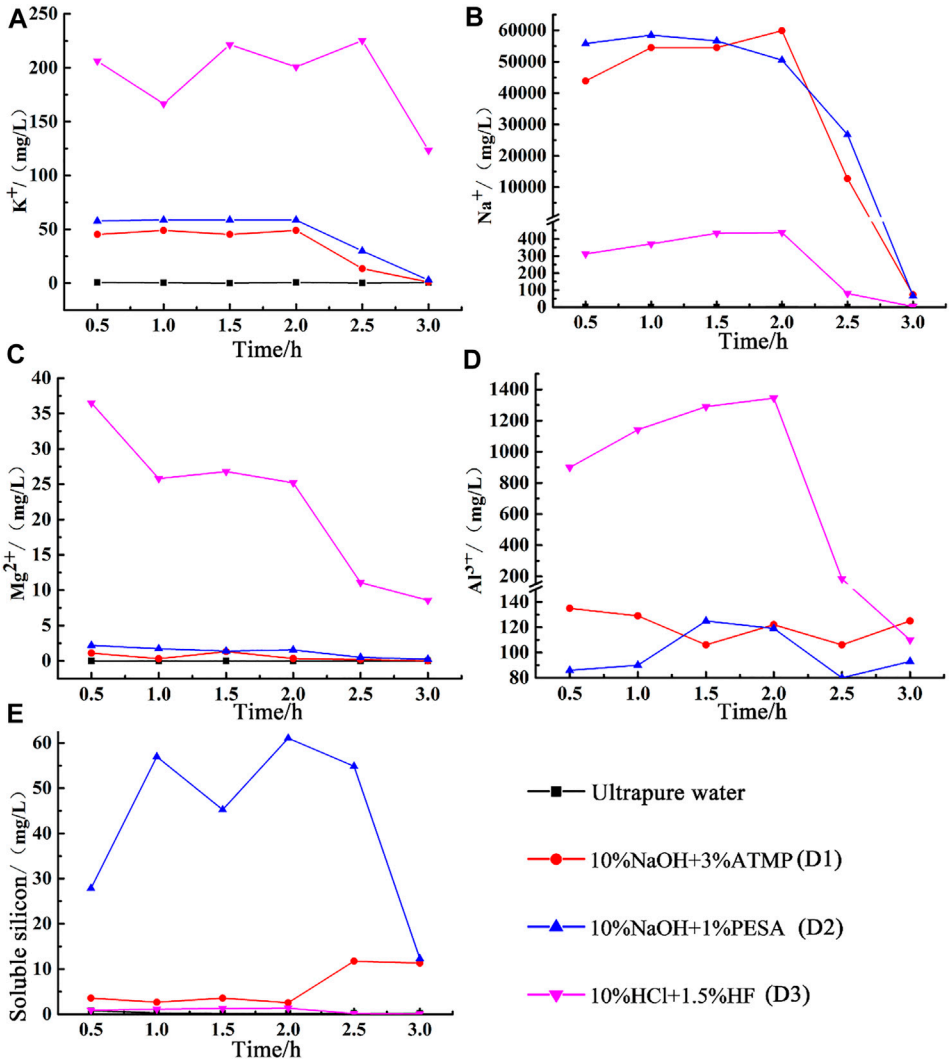

FIGURE 6 | Changes of chemical composition of the dynamic experiment. **(A)** Concentration of K^+; **(B)** concentration of Na^+; **(C)** concentration of Mg^{2+}; **(D)** concentration of Al^{3+}; **(E)** concentration of soluble silicon.

value. The effectiveness of the treatment based on the 10wt% HCl + 1.5wt% HF system was partially ascribed to the small scale of this laboratory experiment, in the sense that the limited length of the core (5 cm) allowed for a complete penetration of the stimulant throughout the specimen. For the same reason, also the particles produced in the early stage of main flush were likely removed by the injected fluid and likely discharged out of the fractured specimen along with the residual acid.

4.2 Reaction Mechanism Analysis of Chemical Stimulation

4.2.1 Changes of Chemical Components of Residual Stimulants

The chemical composition of residual stimulants under dynamic conditions is shown in **Figure 6**. During the injection of ultrapure water, the concentration of the main chemical components in the residual liquid remained close to zero because ultrapure water did not boost any dissolution process. Under this configuration, the observed decline in permeability was, thus, ascribed to the gradual increase in fracture tightness, driven by the high value of the confining pressure (10 MPa).

Very similar Na^+, K^+, Mg^{2+}, and Al^{3+} concentrations patterns were observed in the residual solution when either the 10wt% NaOH + 3wt% ATMP or the 10wt% NaOH + 1wt% PESA systems were used for chemical stimulation. No significant fluctuation in the dissolution rate was observed during the stimulation process, as testified by the invariably low Mg^{2+} concentration (2.2 mg/L and 1.3 mg/L).

Since the increase in Na^+ and K^+ concentration can be ascribed with reasonable confidence to plagioclase and potassium feldspar dissolution processes in our experimental setup and the increase in Mg^{2+} concentration to chlorite dissolution, we claimed that NaOH-dominated alkaline chemical stimulants had the potential

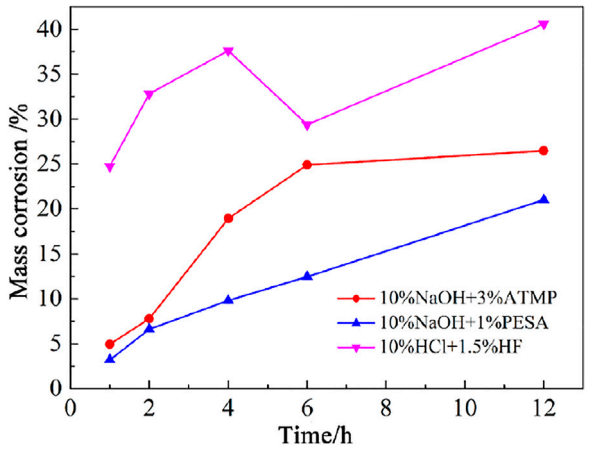

FIGURE 7 | Change of the mass corrosion rate of rock powder.

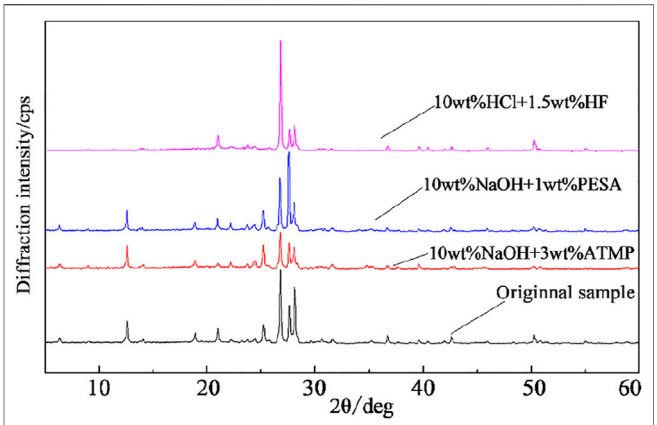

FIGURE 8 | XRD diffraction curves of residual samples after reaction for 12 h.

to slowly dissolve plagioclase and albite, while it had virtually no impact on chlorite stability. From the perspective of the chemical composition of the residual stimulants, the two stimulation schemes manly differed in terms of soluble silicon concentration (**Figure 6E**), a parameter which mirrored differences in quartz dissolution efficiency (see large fluctuation in cores permeability in the late stage of the main flush; **Figure 5**).

Similar and relatively high Na^+, K^+, and Al^{3+} concentrations were observed in the reaction residue after treatment with both NaOH-dominated alkaline and the 10wt% HCl + 1.5wt% HF acid solutions. Na^+ concentration increased gradually in the whole main flush stage, and the concentration of K^+ fluctuated between 174.2 and 227.5 mg/L, reflecting the capacity of these stimulants to induce substantial dissolution of feldspar and plagioclase. Mg^{2+} concentration increased up to about 36.5 mg/L at the beginning of the main stage and then gradually decreased with the progress of the experiment.

Based on differences in Mg^{2+} concentration, we noticed that under dynamic conditions, the 10wt% HCl + 1.5wt% HF configuration showed the best performance in terms of chlorite dissolution efficiency, in agreement with the recognized acid-sensitive behavior of chlorite (e.g., Tang et al., 2007; Kamal et al., 2019). The unexpected low Mg^{2+} concentration produced during this experiment was then interpreted as an effect of the low initial content of chlorite in the processed specimen.

With an average of only about 0.8 mg/L, the soluble silicon concentration did not increase significantly, reflecting the scarce reactivity of quartz with respect to low-concentration mud acids. Similar conclusions have been drawn in other studies based on evidences from scanning electron microscope analysis (Guo et al., 2020).

Overall, we noted that the 10wt% HCl + 1.5wt% HF configuration preferentially affect, reducing it, feldspar and chlorite concentration, leaving almost intact the primary quartz fraction. The initial increase in permeability noticed during the early stage of the main flush was then attributed to the availability of fresh, reactive surface area of primary feldspar and chlorite. As soon as the interaction progressed, this area progressively reduced, and the equivalent permeability first started to oscillate and then gradually stabilized in the post-flush stage.

4.2.2 Results of Prolonged Static Corrosion experiment

4.2.2.1 Sample Corrosion

The time variation of the dissolution rate of the rock samples under static conditions is shown in **Figure 7**. A gradual increase in the dissolution rate was observed when granite specimens were allowed to react with both 10wt% NaOH + 3wt% ATMP and 10wt % NaOH + 1wt% PESA agents, with the only relevant difference between the two experimental setups that under 10wt% NaOH + 3wt% ATMP conditions, some flattening of this trend was noticed after 4 h reaction time. Under 10wt% NaOH + 1wt% PESA conditions, dissolution patterns flattened after 2 h. It emerged that PESA was an effective chelating agent when associated with alkaline chemical stimulants.

Different from the results of the dynamic stimulation experiment, under static conditions, the 10wt% NaOH + 3wt% ATMP agent turned out to be very effective in driving the dissolution of primary minerals. This behavior was tentatively explained in terms of the dependency of the performance of NaOH-dominated alkaline stimulants on the hydrodynamic conditions of the fracture (Guo et al., 2020). In particular, it has been observed that the occurrence of an irregular flow of the stimulant may led to the accumulation of small mineral particles within the fracture, resulting in a decline of the equivalent permeability of the core. The application of the 10wt% NaOH + 1wt% PESA agent was then associated with a lesser accumulation of particles in the fracture that finally resulted in a more efficient reservoir reconstruction, compared to the 10wt% NaOH + 3wt% ATMP case.

The 10wt% HCl + 1.5wt% HF acid system efficiently performed (i.e., better than alkaline stimulants) during the first stage of the reaction path, up to a maximum dissolution rate of

TABLE 3 | XRD results after reaction for 12 h (%).

Scheme number	Quartz	K-Feldspar	Plagioclase	Chlorite	Biotite	Amorphous state
Original sample	20	30	33	15	2	—
S1	13	22	15	15	2	33
S2	15	51	17	15	2	—
S3	40	23	16	—	2	19

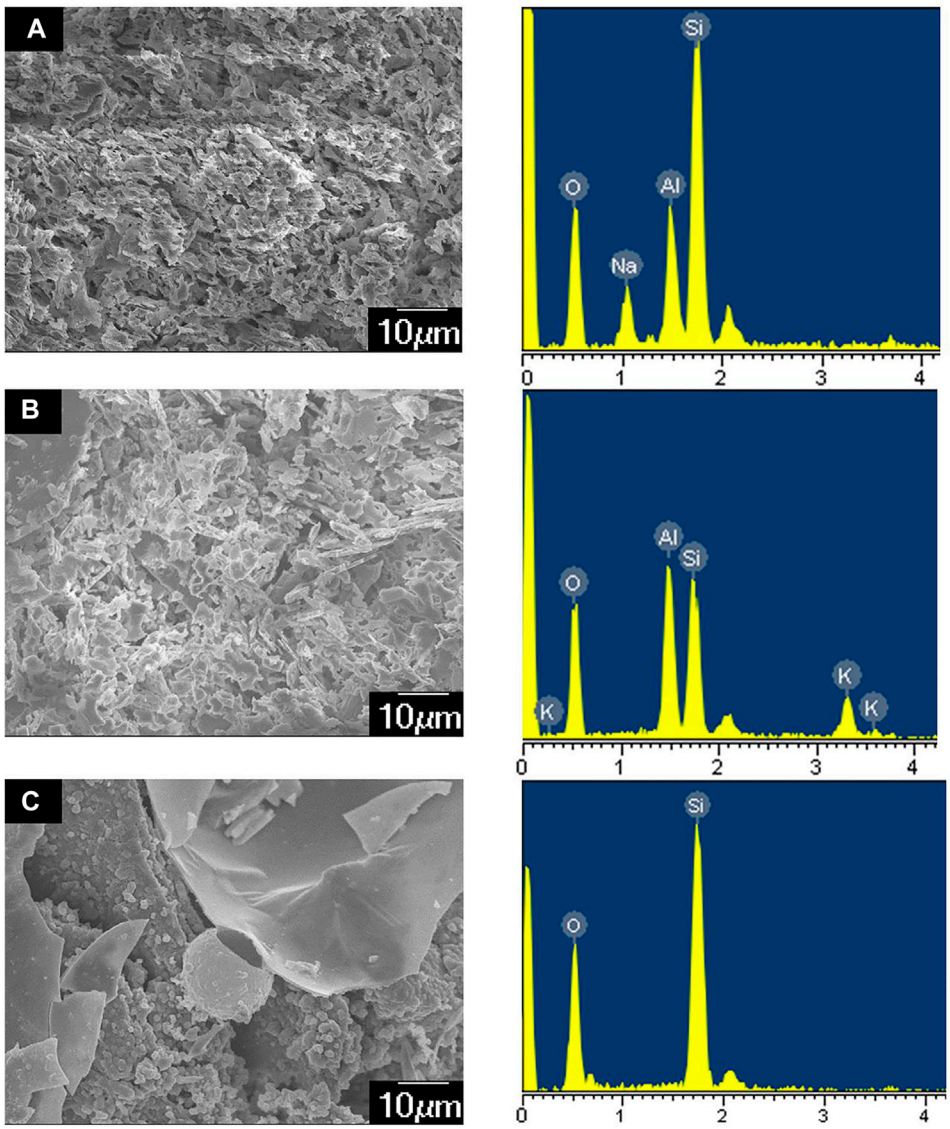

FIGURE 9 | SEM images of secondary precipitation. **(A)** Secondary plagioclase; **(B)** secondary potassium feldspar; **(C)** amorphous silica.

37.6% after 4 h interaction. Then, a minimum value of 29.4% was estimated after 6 h. A relatively large amount of secondary precipitates was observed during this time interval. According to XRD results (**Figure 8** and **Table 3**) and scanning electron microscope tests (**Figure 9**), during this stage, the main newly formed solids were quartz and amorphous silica. The mass dissolution rate of primary minerals increased again during the 6–12 h time span, up to the maximum value of 40.6% after 12 h of reaction. These features indicated that the dissolution effect driven by the stimulant overwhelmed the

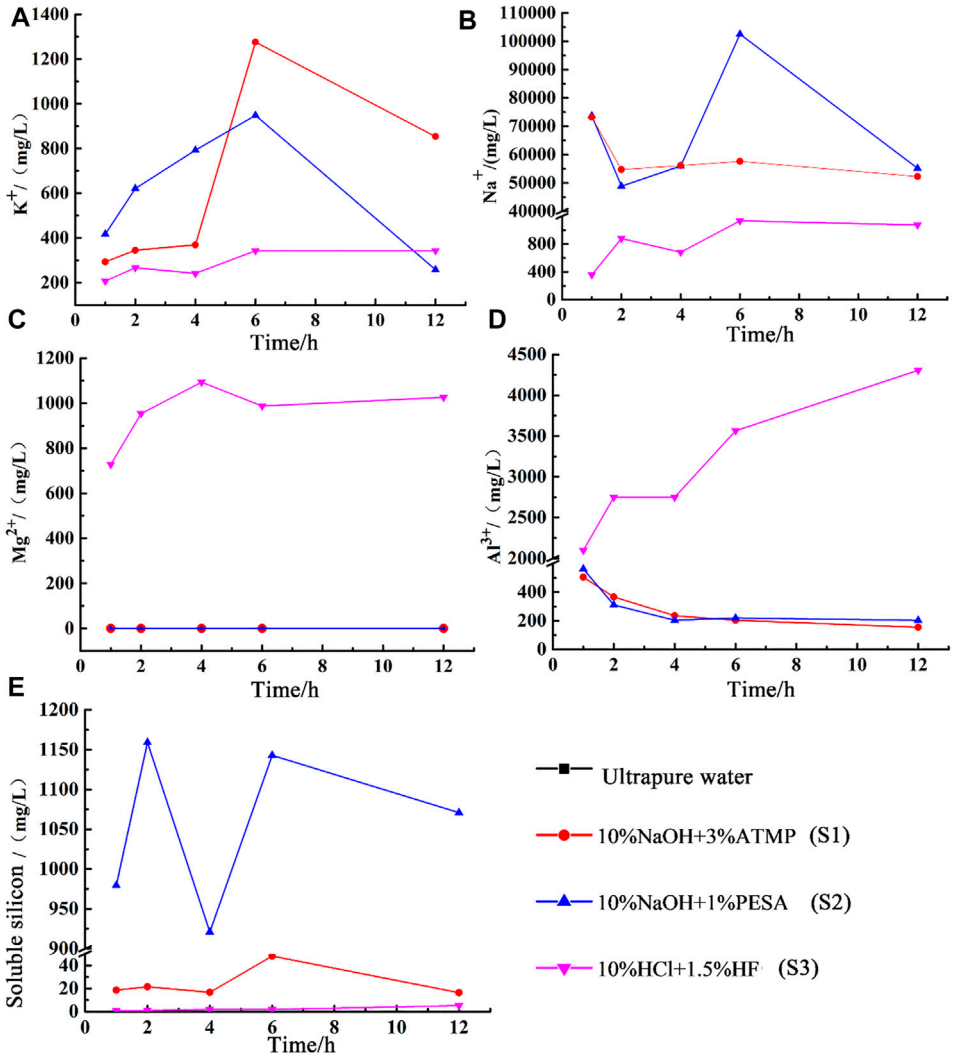

FIGURE 10 | Changes of chemical composition of the static experiment. **(A)** Concentration of K^+; **(B)** concentration of Na^+; **(C)** concentration of Mg^{2+}; **(D)** concentration of Al^{3+}; **(E)** concentration of Soluble silicon.

counter effect of the formation of secondary mineral/amorphous phases, testifying about the effectiveness of this formula.

4.2.2.2 Chemical Composition of Residual Stimulants

The chemical composition of residual stimulants under static conditions is shown in **Figure 10**. K^+ concentration increased during the first 2-h reaction when 10wt% NaOH + 3wt% ATMP and 10wt% NaOH + 1wt% PESA configurations were used, while Na^+ and Al^{3+} concentrations showed a minor decrease, indicating the possible formation of secondary plagioclase. The concentration of Na^+ and K^+ in the 10wt% NaOH + 3wt% ATMP residue increased significantly during the 2–6h interval, while the Na^+ and K^+ concentration increased slightly in the 10wt% NaOH + 1wt % PESA residue. After 12h, Na^+, K^+, and Al^{3+} concentrations decreased significantly in the 10wt% NaOH + 1wt% PESA case. Combined with XRD and SEM results (**Figure 10A**), these evidences were interpreted as an indication for K-feldspar and plagioclase precipitation. Conversely, during the same period, negligible feldspar dissolution/precipitation was observed under the 10wt% NaOH + 3wt% ATMP configuration.

XRD results and chemical patterns of **Figure 10C** indicated that the very low Mg^{2+} residual concentration associated with the interaction with alkaline agents likely mirrored the very low reactivity of chlorite under these experimental conditions.

Silicon emerged as a key parameter to trace variable quartz dissolution rates under alkaline conditions. As shown in **Figure 10E**, the soluble silicon concentration in the 10wt% NaOH + 1wt% PESA reaction residue was set up to 921–1143 mg/l, whereas it did not exceed 16.5–48.1 mg/l under 10wt% NaOH + 3wt% ATMP conditions.

When 10wt% HCl + 1.5wt% HF was used as the stimulant, the concentrations of K^+, Na^+, and Mg^{2+} showed an overall upward trend in the first 6 h of the reaction, with Na^+ being the only element decreasing over the 2–4 h interval. It is noteworthy that

the sample dissolution rate increased by 4.8% during this period. Combined with the change in Mg^{2+} concentration and with XRD results, chlorite dissolution was identified as the most relevant mineralogical transformation associated with this stage. The concentration of K^+ decreased significantly over the 6–12 h interval. It is speculated that a certain amount of K-feldspar precipitation was produced during this period. While K^+ concentration fluctuates greatly (**Figures 10A,B**), Na^+ concentration did not change significantly after 2 h, suggesting a relatively fast stabilization of albite.

Figure 10C shows that chlorite effectively dissolved upon reaction with 10wt% HCl + 1.5wt% HF, but the dissolution rate decreased gradually over time due to the decrease of chlorite content and the increase of ion concentration in the residual solution. The direct relationship between the progressively reduced amount of primary chlorite and the decrease of its dissolution rate was related to the fact that the overall dissolution rate of each mineral is directly proportional to its total reactive surface area, which in turns linearly depends on the total amount of the mineral and on its specific reactive area (e.g., Lasaga, 1984). As a result, the dissolution effect of the stimulant gradually weakens during the advancement of the reaction. **Figure 10E** indicates that despite a steady tendency to increase over time, silicon concentration remained at low concentration values (5.3 mg/l at 12 h) after interaction with 10wt% HCl + 1.5wt% HF. This chemical stimulant had a very limited dissolution capacity on quartz, consistent with experimental evidences from the literature (Luo et al., 2018).

To sum up, NaOH-dominated alkaline stimulants had the potential to slightly dissolve feldspar and quartz in the fractures, but they were not able to dissolve chlorite. The main difference in the performance of the two alkaline configurations can be recast in terms of a different impact on quartz concentration and formation of secondary minerals. The 10wt% HCl + 1.5wt% HF acid system is more effective in dissolving primary feldspar and chlorite, but this mechanism has the side effect of inducing the precipitation of significant amounts of secondary quartz.

4 CONCLUSION

Laboratory experiments were conducted on cylindrical granite samples from Baimiao formation to characterize its coupled hydraulic and geochemical response to chemical stimulation with different agents. The emphasis was on the static and dynamic behavior of the granite under T,P conditions (150°C, 10 MPa) relevant for the possible development of an EGS in the Matouying uplift area (Hebei Province, China). The main conclusions are as follows.

1) Acid stimulants based on HF and HCl performed better than NaOH-based alkaline agents to enhance the permeability of Baimiao granite cores. In particular, the 10wt% HCl + 1.5wt% HF configuration led to a maximum permeability increase of more than 27 times and the 10wt% NaOH + 1wt% PESA configuration to an increase of about 2.8 times, while the 10wt % NaOH + 3wt% ATMP agent did not show any impact on core permeability.
2) NaOH-dominated alkaline stimulants led to only minor feldspar and quartz dissolution. These agents induced the formation of secondary plagioclase but did not induce any chlorite dissolution. Alkaline chemical stimulants coupled with different chelating agents had variable impacts on quartz dissolution and precipitation of secondary phases. PESA emerged as the best-performing chelating agent to be coupled with NaOH-based alkaline stimulants.
3) The 10wt% HCl + 1.5wt% HF acid system showed significant potential to dissolve primary feldspar and chlorite of the Baimiao granite. Under laboratory conditions, this process was accompanied by relatively large amounts of newly formed amorphous silica, which were unaccompanied by an equivalent dissolution of primary quartz. This chemical agent proved to be effective in reconstructing the target rock, and under field conditions, its penetration performance can be likely optimized through the combined use of corrosion inhibitors and other components that might enhance its inhibition speed.

Overall, the laboratory experiments of this study set the baseline for the assessment of the field performance of a possible chemical stimulation program in a granite-hosted EGS reservoir. However, due to scale effects and the inherent complex distribution of fractures under field conditions, these results should be considered a preliminary support reference frame. Site-scale numerical simulations and field tests need to be carried out in the follow-up research to complement the current experimental approach.

DATA AVAILABILITY STATEMENT

The original contributions presented in the study are included in the article/Supplementary Material, further inquiries can be directed to the corresponding author.

AUTHOR CONTRIBUTIONS

SS and XQ completed the collection of regional data and the collection and preparation of the samples; BF and GF provided the overall idea and schemes; SH and JX completed part of the experiment; and ZC completed part of the experiment and finished this manuscript.

FUNDING

This work was jointly supported by the National Key R&D Program of China (No. 2018YFB1501802), Key Department Construction Project of Hebei Bureau of Coal Geological Exploration (No.205A4101H), Single Well Heat Extraction and Surface Comprehensive Heat Utilization Technology of HDR (No.19274102D), and College of New Energy and Environment

of the Jilin University and the Institute of Geosciences and Earth Resources (IGG) of the National Council of Italy (CNR) partnered in the Frame of the MOD-GRE (MODelling Conventional and Unconventional Geothermal Resources in Italy and China) Collaborative Project, Jilin Province Science and Technology Development Project (Grant No. 20200403147SF).

REFERENCES

Alegria, P., Catalan, L., Araiz, M., Rodriguez, A., and Astrain, D. (2022). Experimental Development of a Novel Thermoelectric Generator without Moving Parts to Harness Shallow Hot Dry Rock Fields. *Appl. Therm. Eng.* 200, 117619. doi:10.1016/j.applthermaleng.2021.117619

Davies, D. R., Faber, R., Nitters, G., and Ruessink, B. H. (1994). A Novel Procedure to Increase Well Response to Matrix Acidising Treatments. *SPE Adv. Technol. Ser.* 2 (1), 5–14.

Economides, M. J., and Nolte, K. G. (1989). *Reservoir Stimulation*. 2nd ed. Upper Saddle River, NY, USA: Prenitce Hall, 440.

Evanoff, J., Yeager, V., and Spielamn, P. (1997). Stimulation and Damage Removal of Calcium Carbonate Scaling in Geothermal Wells: A Case Study. *Energ. Sourc.* 19 (1), 2481–2485.

Feng, B., Xu, J., Xu, T., Li, S., Song, D., and Chen, M. (2019). Application and Recent Progress of Chemical Stimulation on Hot Dry Rock Reservoir Modification. *J. Earth Sci. Environ.* 41 (5), 577–591. doi:10.3969/j.issn.1672-6561.2019.05.006

Guo, Q., He, T., Zhuang, Y., Luo, J., and Zhang, C. (2020). Expansion of Fracture Network in Granites via Chemical Stimulation: A Laboratory Study. *Earth Sci. Front.* 27 (1), 159–168. doi:10.13745/j.esf.sf.2019.12.2

Kamal, M. S., Mahmoud, M., Hanfi, M., Elkatatny, S., and Hussein, I. (2019). Clay Minerals Damage Quantification in sandstone Rocks Using Core Flooding and NMR. *J. Petrol. Explor Prod. Technol.* 9 (1), 593–603. doi:10.1007/s13202-018-0507-7

Lasaga, A. (1984). Chemical Kinetics of Water-Rock Interactions. *J. Geophys. Res.* 89, 4009–4025. doi:10.1029/JB089iB06p04009

Liao, Z., Zhang, Y., Chen, W., Peng, Z., and Xiong, X. (2006). Available Persist Exploitation and Utilization of Geothermal Resourses. *China Mining Mag.* 15 (10), 8–11. doi:10.3969/j.issn.1004-4051.2006.10.003

Liu, M., Zhuang, Y., Zhou, C., Zhu, M., Zhang, C., Zhu, Y., et al. (2016). Application of Chemical Stimulation Technology in Enhanced Geothemal System: Theory, Practice and Expectation. *J. Earth Sci. Environ.* 38 (2), 267–276. doi:10.3969/j.issn.1672-6561.2016.02.014

Luo, J., Zhu, Y., Guo, Q., Tan, L., Zhuang, Y., Liu, M., et al. (2018). Chemical Stimulation on the Hydraulic Properties of Artificially Fractured Granite for Enhanced Geothermal System. *Energy* 142, 754–764. doi:10.1016/j.energy.2017.10.086

Na, J., Xu, T., Wu, Y., Feng, B., and Bao, X. (2017). Effectiveness of Using Mud Acid as Stimulation Agent for Enhanced Geothermal Systems (EGS) Reservoir. *J. Cent. South Univ. (Science Technology)* 48 (1), 247–254. doi:10.11817/j.issn.1672-7207.2017.01.033

Na, J., Feng, B., Lan, C., Xu, T., and Bao, X. (2014). Effectiveness of Using Supercritical CO2 as Stimulation Agent for Enhanced Geothermal Systems. *J. Cent. South Univ. Technol.* 45, 2447–2458.

Olasolo, P., Juárez, M. C., Morales, M. P., D´Amico, S., and Liarte, I. A. (2016). Enhanced Geothermal Systems (EGS): A Review. *Renew. Sustain. Energ. Rev.* 56, 133–144. doi:10.1016/j.rser.2015.11.031

Perthuis, H., Touboul, E., and Plot, B. (1989). "Acid Reactions and Damage Removal in Sandstones: A Model for Selecting the Acid Formulation," in SPE International Symposiumon Oilfield Chemistry, Houston, Texas, February 8–10, 1989 (Houston: Society of Petroleum Engineers). doi:10.2118/18469-ms

Portier, S., and Vuataz, F. D. (2010). Developing the Ability to Model Acid-Rock Interactions and Mineral Dissolution during the RMA Stimulation TEST Performed at the Soultz-Sous-Forêts EGS Site, France. *Comptes Rendus Geosci.* 342 (7/8), 668–675. doi:10.1016/j.crte.2010.04.002

Portier, S., Vuataz, F.-D., Nami, P., Sanjuan, B., and Gérard, A. (2009). Chemical Stimulation Techniques for Geothermal Wells: Experiments on the Three-Well EGS System at Soultz-Sous-Forêts, France. *Geothermics* 38, 349–359. doi:10.1016/j.geothermics.2009.07.001

Qi, X., Zhang, G., Shangguan, S., Su, Y., Tian, L., Li, X., et al. (2018). A Brief Analysis of Hot and Dry Rock Geothermal Resource Hosting and Distribution in Hebei Province. *Coal Geology. China* 30 (11), 47–73. doi:10.3969/j.issn.1674-1803.2018.11.11

Qi, X., Shangguan, S., Zhang, G., Pan, M., Su, Y., Tian, L., et al. (2020). Site Selection and Developmental Prospect of a Hot Dry Rock Resource Project in the Matouying Uplift,Hebei Province. *Front. Earth Sci.* 27, 94–102. doi:10.13745/j.esf.2020.1.11

Sarda, J. P. (1977). "Chemical Leaching," in The 2nd NATA-CCMS Information Meeting on Hot Dry Rock Geothermal Entergy, Los Alamos, NM, United States, June 28–30, 1977 (Los Alamos: Institute of Geophysics ETH Zurich).

Schechter, R. S. (1992). *Oil Well Stimulation*. Englewood Cliffs, NJ, USA: Prentice-Hall, 640.

Shangguan, S. (2017). Occurrence Conditions of Hot-Dry-Rock Geothermal Resources and Development Prospects in Matouying Area. *China Energ. Environ. Prot.* 39 (5), 155–165. doi:10.19389/j.cnki.1003-0506.2017.05.032

Smith, C. F., and Hendrickson, A. R. (1965). Hydrofluoric Acid Stimulation of sandstone Reservoirs. *J. Pet. Technol.* 17, 215–222. doi:10.2118/980-pa

Tang, H., Zhao, F., Li, G., Wang, C., and Xie, X. (2007). Experimental Study on the Reaction of Chlorite with Mud and Fluoroboric Acids. *Oilfield Chem.* 24 (4), 307–309. doi:10.19346/j.cnki.1000-4092.2007.04.005

Wang, G., Liu, Y., Zhu, X., and Zhang, W. (2020). The Status and Development Trend of Geothermal Resources in China. *Earth Sci. Front.* 27 (01), 1–9.

Wang, J., Huang, S., Huang, G., and Wang, J. (1990). *Basic Characteristics of Geothermal Distribution in China*. Beijing: Seismological Press.

Wang, X., Wu, N., Su, Z., and Zeng, Y. (2012). Progress of the Enhanced Geothermal systems(EGS)development Technology. *Prog. Geophys.* 27 (1), 355–362. doi:10.6038/j.issn.1004-2903.2012.01.041

Xu, J. (2005). China's Geothermal Resources and its Sustainable Development and Utilization. *China Popul. Resour. Environ.* 15 (2), 139–141. doi:10.3969/j.issn.1002-2104.2005.02.032

Xu, T., Hu, Z., Li, S., Jiang, Z., Hou, Z., Li, F., et al. (2018). Enhanced Geothermal System: International Progress and Research Status of China. *Acta Geologica Sinica* 92 (09), 1936–1947. doi:10.3969/j.issn.0001-5717.2018.09.012

Yang, F. (2012). *Acidizing Sandstone Reservoirs Using HF and Organic Acids*. College Station, Texas: Texas A&M University.

Yue, G., Li, X., Gan, H., and Wang, G. (2020). A Study on the Reaction Kinetics of Regular Mud Acid and Granite. *Acta Geol. Sin.* 94, 2108–2114. doi:10.19762/j.cnki.dizhixuebao.2020214

Zhang, B., Li, Y., Gao, J., Wang, G., Li, J., Xing, Y., et al. (2020). Genesis and Indicative Significance of Hot Dry Rock in Matouying, Hebei Province. *Acta Geologica Sinica* 94 (7), 2036–2051. doi:10.3969/j.issn.0001-5717.2020.07.012

Conflict of Interest: The authors declare that the research was conducted in the absence of any commercial or financial relationships that could be construed as a potential conflict of interest.

Publisher's Note: All claims expressed in this article are solely those of the authors and do not necessarily represent those of their affiliated organizations, or those of the publisher, the editors and the reviewers. Any product that may be evaluated in this article, or claim that may be made by its manufacturer, is not guaranteed or endorsed by the publisher.